

# Actin Remodeling and Polymerization Forces Control Dendritic Spine Morphology

Karsten Miermans<sup>\*1</sup>, Remy Kusters<sup>1</sup>, Casper Hoogenraad<sup>3</sup>, and Cornelis Storm<sup>1,2</sup>

<sup>1</sup>*Theory of Polymers and Soft Matter, Department of Applied Physics, Eindhoven University of Technology*

<sup>2</sup>*Institute for Complex Molecular Systems, Eindhoven University of Technology*

<sup>3</sup>*Cell Biology, Faculty of Science, Utrecht University*

May 25, 2022

## Abstract

**Keywords:** biophysics | neuroscience | synapse | synaptic plasticity | structural plasticity | filopodium | dendritic spine | cytoskeleton | canham helfrich | actin

Dendritic spines are small membranous structures that protrude from the neuronal dendrite. Each spine contains a synaptic contact site that may connect its parent dendrite to the axons of neighboring neurons. Dendritic spines are markedly distinct in shape and size, and certain types of stimulation prompt spines to evolve, in fairly predictable fashion, from thin nascent morphologies to the mushroom-like shapes associated with mature spines. This striking progression is coincident with the (re)configuration of the neuronal network during early development, learning and memory formation, and has been conjectured to be part of the machinery that encodes these processes at the scale of individual neuronal connections. It is well established that the structural plasticity of spines is strongly dependent upon the actin cytoskeleton inside the spine. A general framework that details the precise role of actin in directing the transitions between the various spine shapes is lacking. We address this issue, and present a quantitative, model-based scenario for spine plasticity validated using realistic and physiologically relevant parameters. Our model points to a crucial role for the actin cytoskeleton. In the early stages of spine formation, the interplay between the elastic properties of the spine membrane and the protrusive forces generated in the actin cytoskeleton propels the incipient spine. In the maturation stage, actin remodeling in the form of the combined dynamics of branched and bundled actin is required to form mature, mushroom-like spines. Our model identifies additional factors that plausibly aid the stabilization and maintenance of spine morphology. Taken together, our model provides unique insights into the fundamental role of actin remodeling and polymerization forces during spine formation and maturation.

## 1 Introduction

A single neuron can contain hundreds to thousands of dendritic spines, actin-rich, micron-sized protrusions which project from dendritic shafts [14]. Mature spines consist of two basic compartments: a constricted region called the *neck*, supporting a bulbous *head* containing the postsynaptic site that makes contact with the axon of a nearby neuron. Spines come in a wide range of sizes and shapes, their lengths varying between  $0.2-2\ \mu\text{m}$  and their volumes between  $0.001-1\ \mu\text{m}^3$ . Electron microscopy

---

\*Corresponding author, k.miermans@gmail.com

(EM) studies have identified several morphological categories of spines, such as thin, filopodium-like protrusions (‘thin spines’), and spines with a large bulbous head (‘mushroom spines’) [10–12, 14, 19]. Different live cell-imaging techniques have demonstrated that dendritic spines are highly dynamic structures, subject to constant morphological change even after birth.

Table 1: Various ‘ball-park’ figures of dendritic spines.

Code	Quantity	Typical Scale	Source
$N$	Number of actin filaments in spine-head (see supporting information on how this number was estimated)	$\sim 71$	[19]
$R_{\text{base}}$	Radius of the base of the spine (viz. where the spine is connected to the dendritic membrane). This quantity was estimated on the basis of microscopy images published by [33].	$\sim 300$ nm	[33]
$R_{\text{neck}}$	Radius of a typical spine-neck	$75 \pm 30$ nm	[12]
$R_{\text{head}}$	Radius of a typical spine-head	$220 \pm 154$ nm	[12]
$\mathcal{L}_{\text{neck}}$	Length of a typical spine-neck	$0.2 - 2$ $\mu\text{m}$	[33]
$\mathcal{L}_{\text{filop.}}$	Length of a typical filopodium	$0.9 - 10$ $\mu\text{m}$ [6] (mean $\approx 5$ $\mu\text{m}$ [39])	[6, 39]
$\ell$	Length that actin filament extends upon one polymerization step	$2.2$ nm	[21]
$\mathcal{A}_{\text{neck}}$	Surface-area of a typical spine-neck	$0.24 \pm 0.17$ $\mu\text{m}^2$	[12]
$\mathcal{A}_{\text{head}}$	Surface-area of a typical spine-head	$0.61 \pm 0.57$ $\mu\text{m}^2$	[12]
$\mathcal{A}_{\text{filop.}}$	Surface-area of a typical filopodium (this was calculated using $\mathcal{A}_{\text{filop.}} \approx 2\pi R_{\text{filop.}} \mathcal{L}_{\text{filop.}}$ with $R_{\text{filop.}}, \mathcal{L}_{\text{filop.}}$ from [6, 39])	$0.85 - 16$ $\mu\text{m}^2$ (mean $\approx 6.3$ $\mu\text{m}^2$ )	[6, 39]
$f_{\text{neck}}$	Expansive force that a spine-neck of typical size exerts (using the approximate formula $f_{\text{neck}} \approx 4\pi K_b R_{\text{head}} / R_{\text{neck}}^2$ , see text)	$9 - 290$ pN	
$f_{\text{head}}$	Contractile force that a spine-head of typical size exerts (using the approximate formula $f_{\text{head}} \approx 17.23 K_b R_{\text{neck}} / \mathcal{A}_{\text{head}}$ , see text)	$0.0007 - 0.05$ pN	
$f_{\text{actin}}$	Average actin polymerization force	$3.8$ pN	[21]
$K_b$	Bending rigidity of lipid bilayer membrane	$5 \times 10^{-19}$ J	[28]

During neuronal development, dendrites initially appear as thin and hairlike filopodia (figure 1). They are defined as having a length that is at least twice the width, and they do not display the bulbous head found on dendritic spines [17, 19, 37]. Filopodia are devoid of organelles and vesicles, and are composed primarily of actin filaments. These actin filaments are bundled and primarily aligned to the nascent spine. Filopodia are the precursors to dendritic spines, and their flexibility allows the establishment of synaptic contacts. Once the contact between a dendritic filopodium and a neighboring axon has been established, the spine-head begins to swell, taking on a more mushroom-like morphology. Over time, such recognizable mushroom spines become the prevalent structure on the dendritic shaft, and few filopodia remain.

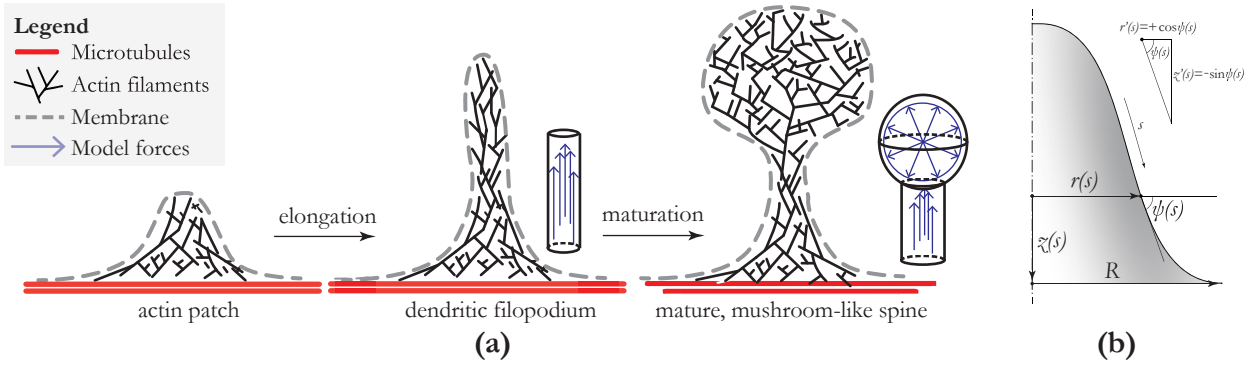


Figure 1: Outline of the model for spine formation and maturation. Panel (a): Cartoon of spine initiation, elongation and maturation. From left to right: ‘stubby spines’; dendritic filopodia or thin spines; mature, mushroom-like spines. In our mathematical model, we solve the shape equation based on the energy functional (1) (see SI, equation (3)). In this study we show that, at least for the purposes of the force calculations, the results of the shape equation can be reproduced using the geometries that are also displayed in this figure. Panel (b): Definition of axisymmetric coordinate system that use for our models.

The progressive shape change is neither random nor deterministic. Rather, it is thought to be correlated with the strength and maturity of each synapse [17, 37]. At the level of an individual spine, strengthening of a synapse is accompanied by modifications in the size of the spine. The prime mechanisms that drives structural plasticity is the modulation of actin dynamics in dendritic spine. Although the importance of actin remodeling as well as the synaptic signaling mechanisms involved in structural synaptic plasticity are well established [14, 19, 23], a general framework to correlate the state of the actin cytoskeleton to spine shape is lacking. Most importantly, it is not clear whether the actin is capable of autonomously *driving* the shape change, or whether the actin simply *follows* morphological transitions otherwise imposed.

Our model for spine dynamics uses the Canham-Helfrich formalism, an approach which has proven its strength in describing, both qualitatively and quantitatively, the deformation of biological membranes in numerous biological systems such as red-blood cells [1], membrane tethers [3] and binary or tertiary lipid mixtures in giant-unilamellar vesicles [28]. For a broad overview, we refer to [27] and many references therein. We analyze the interplay of the plasma membrane with the underlying actin cytoskeleton to quantify the forces that are required to prompt the initial formation of the spine, and its subsequent outward growth. We find that the forces generated by actin polymerization are sufficient for it to drive filopodium formation, and that the resulting dimensioning (quantified, for instance, by the ratio (protrusion width)/length) closely resembles those reported in experiments. A related theoretical model taking into account the interplay of the spine membrane with the actin cytoskeleton allows us, in addition, to compute the forces and energies required for spine head formation. It shows that the simultaneous presence of both branched actin filaments and bundled/aligned actin is required, and sufficient, to produce the typical mushroom-like spine morphology. Finally, our model also highlights the important role of additional physical processes in stabilizing the morphological features of mature spines. We discuss several candidate factors that may effect these processes, and conclude that these molecules are sufficiently rigid to be able to constrict the spine-neck to the extent reported in experiments. Our models do point to a fundamental role for actin remodeling in the process of spine formation and maturation. This finding supports earlier claims in the literature, and our model suggests novel experiments to further pin down the basic principles that control the structural plasticity of the brain.

## 2 Materials and Methods

Reflecting the approximate rotational symmetry of dendritic spines, we use an axisymmetric coordinate system consisting of an angle  $\psi$  with the horizontal, an arc-length parameter  $s$ , radial coordinate  $r$  and vertical coordinate  $z$ . The coordinate system is schematically displayed in figure 1. The arc-length parameter  $s = 0 \dots \mathcal{S}$  is used as the independent variable and  $r(s)$  and  $\psi(s)$  as the coordinates. This coordinate system fully determines the shape, and the vertical coordinate  $z(s)$  is recovered by the geometrical relation  $z'(s) = -\sin \psi(s)$ . The Canham-Helfrich energy functional that we use can be written [3, 28]

$$\mathcal{F} = \frac{1}{2}K_b \int da (2H)^2 + \sigma(\mathcal{A} - \mathcal{A}_0) - f(\mathcal{L} - \mathcal{L}_0), \quad (1)$$

where  $K_b \approx 500 \text{ pN} \cdot \text{nm}$  is the bending rigidity of the membrane [28],  $2H = \psi'(s) + \sin \psi(s)/r(s)$  is the mean curvature [16] (with  $\psi'(s) \equiv d\psi/ds$ ),  $\sigma$  is a surface tension,<sup>1</sup>  $\mathcal{A} = \int da$  is the surface area,  $f$  is a point-force acting on the membrane and  $\mathcal{L} = z(\mathcal{S}) - z(0)$  is the height of the membrane. The first term in this energy functional—the one containing the mean curvature  $2H$ —represents the bending energy of the membrane, which reflects the tendency of lipid bilayers to adopt a flat shape (or spherical in the case of vesicles). We use the surface tension  $\sigma$  and point-force  $f$  as Lagrange multipliers to enforce specific values of the surface-area  $\mathcal{A}_0$  and the height of the shape  $\mathcal{L}_0$  [30]. Within this paradigm, we interpret the surface-area, viz. amount of membrane available to the spine, as a quantity that encodes growth [24, 34]. The height of the shape reflects the cytoskeletal architecture of the spine. Although there is no obvious way of interpreting the surface tension (cf. footnote 1), the point-force  $f$  is simply the mechanical force that is exerted by the cytoskeleton on the spine membrane. One of the main goals of this paper is to investigate whether these forces are attainable through actin polymerization. We will show that this is indeed the case.

Our choice to work at fixed total surface-area, rather than fixed surface tension, is inspired by two considerations: (i) Dendrites are finite in size, and the membrane that envelopes the dendritic shaft can only be as small as the underlying cytoskeleton of microtubules [14, 19]—therefore, we cannot regard the surroundings of the spine as a reservoir of freely accessible membrane. Instead, excess membrane needs to be transported, often by means of exocytic trafficking, in order to be available to the spine [24, 34]. (ii) On the dendritic shaft, generally, many spines exist side-by-side. In open boundary settings, such as those employed in [3], area is exchanged with a virtual bath outside the integration domain. In the dendritic shaft, however, no such bath exists as the next spine is likely also growing. Thus, a competition for membrane exists between proximate spines. For this reason, we choose to work with closed boundaries, prohibiting area to leak out of the domain of interest.

We choose to work in a setting in which the amount of membrane available to the spine is conserved, i.e. membrane does not leak away from the shape. We point out that there is biological evidence that cells strive to maintain their surface-tension [3, 9, 25]. Although this empirical fact might seem incompatible with our simulations, the ensembles of constant surface-area and constant surface-tension are—for the purpose of modeling mushroom-like spines—approximately equivalent. The underlying reason for this similarity is simple: the energy corresponding to the surface-tension of a typical spine-head is approximately equal to the bending energy of a typical spine-neck. Hence, for mushroom-like shapes, the two ensembles can be converted to one another by swapping an energy term of the same order of magnitude. We have verified this prediction by comparing various quantitative predictions between the two ensembles.<sup>2</sup> Indeed, the predictions that we make in this paper are valid in both

---

<sup>1</sup>This surface tension is a parameter that is used to enforce the total surface-area (a “Lagrange multiplier”), and can therefore not be interpreted (even though it has the same dimensions) as the surface tension of  $\approx 0.05 \text{ pN/nm}$  that is measured in experiments using e.g. membrane tethers [4, 9, 25].

<sup>2</sup>We have compared predictions of the filopodium width, the number of filaments required to support a filopodium, the neck width of a mature spine and the head width. Of these metrics, the mean values of the predictions in these two ensemble differ 5 – 40%.

ensembles.

Using the Euler-Lagrange formalism, the energy functional (1) can be transformed into a system of differential equations. These shape equations, reproduced in the Supporting Information, have been numerically solved by means of a shooting-and-matching technique for a wide range of parameters  $\mathcal{A}_0, \mathcal{L}_0$  and several sets of boundary conditions (we drop the subscripts to  $\mathcal{A}_0, \mathcal{L}_0$  in the remainder of the paper). We ignore the stretching energy since lipid bilayer membranes can be regarded as approximately inextensible [26]. Also, the pressure-term  $-p\mathcal{V}$  that is often cited in conjunction with the Canham-Helfrich formalism [15, 16, 27] is not applicable since we are discussing a system that is free to exchange cytosol with the environment.

### 3 Results and Discussion

We use the Canham-Helfrich energy functional (1) to model the growth of dendritic spine membranes. The growth sequence is schematically shown in figure 1. We will show that this growth sequence can be explained qualitatively and quantitatively by simple models that incorporate the interaction of the actin cytoskeleton and the spine membrane. To that end, we will first determine how filopodia are formed by application of forces that the cytoskeleton exerts on the spine membrane. Then, we will show that the forces generated by a branched cytoskeleton, located at the top of the spine, will result in a bulbous head and a thin spine-neck. Finally, we will show that actin-membrane anchoring or ring-like molecules are another scenario for constraining a large head and long, thin neck. For the model calculations, we shall make repeated use of the physiologically relevant parameters that we have tabulated (see table 1, Supporting Information).

#### 3.1 Filopodium Formation

It is well known that the actin cytoskeleton plays a large role in the formation of filopodia [14]. It has been hypothesized that polymerization of actin filaments and the resultant forces are sufficient for the formation of dendritic filopodia [2]. In order to theoretically investigate this possibility, we will present a model that includes extension of the actin cytoskeleton in growing filopodia. This is schematically displayed in the outline of our model, figure 2. This is readily incorporated in the energy functional (1) by fixing the height of the shape—thereby representing the vertical dimension of the cytoskeleton. Growth of the cytoskeleton, or change in cytoskeletal architecture, is represented by incrementing this height constraint. We will first show that the forces that this rigid structure needs to exert on the spine membrane match the forces that are generated by actin polymerization. Then, we will show that the sequence of shapes as a consequence of polymerization of the actin cytoskeleton is similar to that of filopodium formation.

The protrusive forces that the rigid actin cytoskeleton exerts on the spine-membrane, will result in tube-like shapes, as can be seen in figure 2. Also shown are the force-extension curves of these tubes for various values of the membrane surface-area. Since growth of dendritic spines and filopodia is mediated by exocytosis of endosomes at the synapse [24, 34], we can model the growth of spines by increasing the surface-area of the shape (also see the Methods part of this paper). Thus, we find that filopodia with more membrane require less force to be extended—in other words, membrane addition will result in further elongation of filopodia. Although the full force-extension relation shown in figure 2 is non-trivial, the linear part for large extensions (i.e. large height  $\mathcal{L}$ ) can easily be understood from a theory that treats these structures as cylinders. From the bending energy of a cylinder (with given surface-area)  $\mathcal{E} = 2\pi^2 K_b \mathcal{L}^2 / \mathcal{A}$  we find that the force  $f \equiv -\partial_{\mathcal{L}} \mathcal{E}$  to extend this cylinder is linear in  $\mathcal{L}$ . Applying this derivative, we find the force for producing filopodia  $f \approx 4\pi^2 K_b \mathcal{L} / \mathcal{A}$ . This approximation turns out to be accurate to within 9% of the computed force-extension curves shown in figure 2 (the error in this approximation decreases as the filopodium height increases). This is markedly different

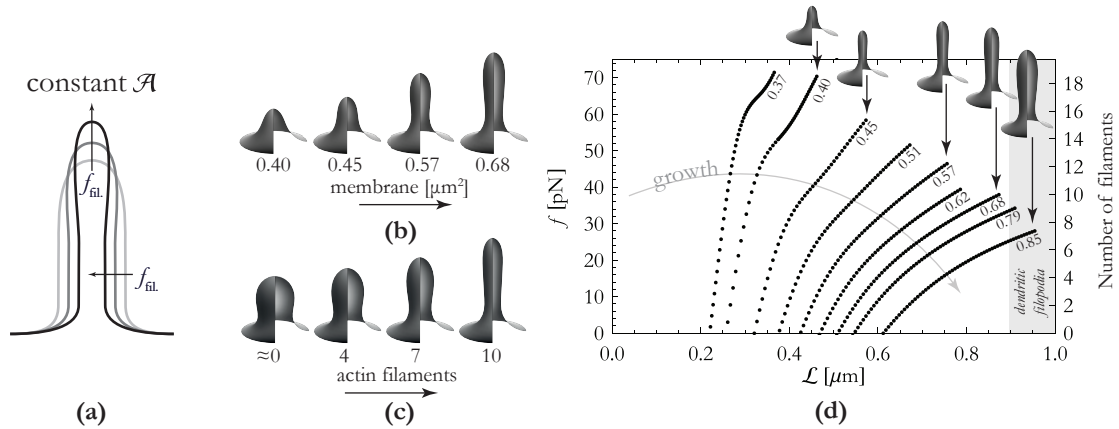


Figure 2: Outline of results for filopodium formation. Panel (a): Cartoon of qualitative effect of increasing force whilst the amount of membrane is kept constant. Panel (b): Effect of growth (viz. membrane addition) on filopodium morphology (if the force on the membrane is kept constant). These shapes experience a vertical force of 35 pN corresponding to approximately 9 polymerizing actin filaments. Membrane addition results in substantial elongation of the filopodium. Panel (c): Effect of cytoskeletal remodelling (viz. actin polymerization) on filopodium morphology if the amount of membrane is kept constant. These shapes have a surface-area of  $0.68 \mu\text{m}^2$ . Increasing the number of polymerizing actin filaments leads to a marked change in morphology from a stubby-like morphology to a tubular shape..

Panel (d): Force-extension curves of our models of dendritic filopodia for various values of the surface-area  $\mathcal{A}$ . Numbers at curves indicate the surface-area in units of  $\mu\text{m}^2$  whereby we used a radius of the base of the filopodia  $R_{\text{base}} = 300 \text{ nm}$ .

from the force required for pulling a tube from a reservoir (i.e. a (quasi-)infinite bath of membrane) of surface area. As is discussed in [3] (using detailed analytical and numerical calculations) the force for pulling a tube from such a reservoir converges to a constant for large extensions. If it were the case, then, that dendritic filopodia were connected to a bath of membrane, we would not expect dendritic filopodia to have a typical length. On the contrary, in that scenario dendritic filopodia would grow *ad infinitum* (given that the applied force is large enough to overcome an initial barrier). We assert that, within the paradigm of a conserved quantity of membrane available to the spine, a finite force will result in a definite length of the filopodia.

As can be seen in figure 2, the force required for formation of dendritic filopodia is in the tens of piconewtons. The polymerization of actin is able to exert, on the average, a force of  $f_{\text{actin}} \approx 3.8$  pN (from [21], see Supplementary Information). We find, using the typical values for the length and surface-area (table 1, see Supporting Information) and the aforementioned formula  $f \approx 4\pi^2 K_b \mathcal{L} / \mathcal{A}$ , a minimal number of actin filaments of 5 – 15. Although we have not been able to find publications that mention the number of actin filaments in dendritic filopodia, examining EM of the cytoskeletal organization of dendritic filopodia from [19] suggests that filopodia typically have 6 – 10 filaments. This comparison tentatively verifies the plausibility of our model for filopodium formation.

Our simulations span up to  $\mathcal{A} = 0.85 \mu\text{m}^2$  and  $\mathcal{L} \approx 950$  nm. Following [6, 39], these shapes can be regarded as relatively small filopodia. Now, measuring the width of the corresponding tubular part of the shape, we find diameters in the order of 160 – 200 nm. Indeed, [12] report values for the diameters of filopodia or thin spines in the range 90 – 210 nm. Thus it is found that the simulations and experimental results have compatible ranges.

### 3.2 The Role of the Actin Cytoskeleton in Spine Maturation

As a consequence of synaptic activity, the spine volume may increase and there is a marked change in the qualitative morphology through formation of a bulbous spine-head [5, 36]. We have previously shown that simply adding membrane to dendritic filopodia results in larger filopodia, but not formation of a bulbous head. Therefore, an additional process is needed in order to produce mature spines. By which mechanisms does this qualitative change in morphology occur? In this part of the paper, we will show that the process of spine maturation can, at least in part, be ascribed to the interaction of the spine membrane with an isotropic actin meshwork.

As is the case for filopodia, it is known that the actin cytoskeleton is intimately linked to the size and shape of the spine head [14, 23], and therefore is essential to understanding spine maturation. By modeling the interaction of the cytoskeleton with the spine membrane, we will investigate the mechanical requirements for a volume increase and morphological transition (that is characteristic of spine maturation) to occur. We will show (by making use of the Canham-Helfrich energy (1) and comparison with experiments) that branched actin filaments in the spine-head are plausibly responsible for the transition from dendritic filopodium to a mushroom-type morphology. Although the models in this paper lack many of the biological details relevant for spine maturation, we find that the forces that are required for spine membrane match the forces that are generated by actin polymerization. Then, we show that typical spine-neck widths are accurately predicted by our models.

An outline of our model for spine maturation is displayed in figure 3. We model the polymerization of actin in the spine-neck as a vertical force and polymerization in the spine-head as a radial force. The discrepancy between these two types of forces stems from the difference in cytoskeletal organization in spines—the spine-head predominantly contains branched actin whereas oriented or linear actin mainly localizes in the spine-neck [14, 19]. This gives rise to an approximately isotropic network of actin in the spine-head, contrary to the actin organization in spine-necks and dendritic filopodia [19]. The polymerization of these two manifestations of actin result respectively in a radial force and a directed force. As is the case for our models for dendritic filopodia, we approximate the total surface-area of the spine as a constant since there is only a finite pool of membrane available on the dendrite (for a more

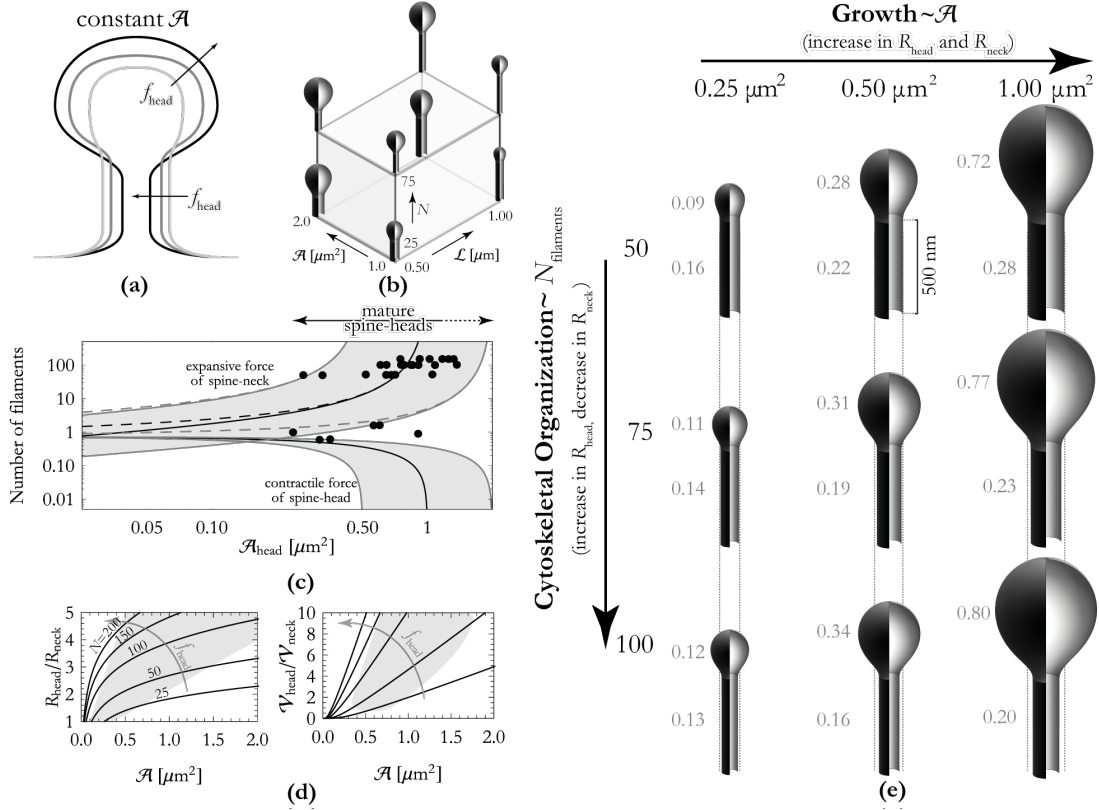


Figure 3: Outline of results for spine maturation. The spine bases have been left out in the renders in this figure. Panel (a): Cartoon showing qualitative effect of increasing force (viz. increasing the number of filaments in the spine-head) whilst the amount of membrane is kept constant. Increasing the number of actin filaments in the spine-head enlarges the spine-head and, at the same time, a thinning neck. Panel (b): Results of our model are combined in a three-dimensional growth-organization matrix, shown here with selected shapes. These shapes show clearly the effects of increasing the number of filaments in the head  $N$ , the total surface-area  $\mathcal{A}$  and the length of the spine-neck  $\mathcal{L}$ . Panel (c): The minimum number of actin filaments required in the cytoskeleton for sustaining the contractile force  $f_{\text{head}}$  that the spine-head membrane exerts and for counteracting the expansive force  $f_{\text{neck}}$  of the spine-neck. Band indicates typical values of the total amount of membrane  $\mathcal{A} = 0.5 \dots 2.0 \mu\text{m}^2$  (cf. table 1). Dashed lines indicate number of actin filaments required for counteracting  $f_{\text{head}} + f_{\text{neck}}$ . Empirical data (black circles) shows reasonable agreement with our model (data taken from [8], see SI). Panel (d): Ratio of head and neck radii (left) and volumes (right) for a number of actin filaments  $N = 25, 50, 100, 150, 200$  (lower to upper curves). For these plots we used equation (2) with  $\mathcal{L}_{\text{neck}} = 500 \text{ nm}$ . Experimental data from [33] is highlighted in gray. Panel (e): Effects of growth (membrane addition) and the number of actin filaments in the spine-head on spine morphology. In these models, we kept the total length of the spine-neck fixed. Dotted lines are a visual aid for showing how increasing the number of actin filaments in the spine-head results decreases the width of the spine-neck.



detailed explanation, see the Methods part of this paper). This approximation, combined with the fact that lipid membranes are practically inextensible [26], leads to the following assertion: exerting an outward force on the spine-head results in the transportation of membrane from the spine-neck to the spine-head. More simply stated, cytoskeletal growth in the spine-head results in an increase of the size of the spine-head at the expense of a decrease in the neck width.

In order to make the above considerations quantitative, we propose a model for the spine membrane that is composed of a cylinder of constant height (but variable radius) connected to a sphere. As displayed in figure 3, we model  $N$  filaments in the spine-head that each apply an outward radial force  $f_{\text{actin}} = f_{\text{head}}/N$  over a radius  $R_{\text{head}}$ . The work performed by this force is  $f_{\text{head}}R_{\text{head}}$ . Likewise, the energy required for attaining a neck of length  $\mathcal{L}_{\text{neck}}$  and radius  $R_{\text{neck}}$  is  $\pi K_b \mathcal{L}_{\text{neck}}/R_{\text{neck}}$  (equation (1)). Balance of forces dictates that the total energy  $\pi K_b \mathcal{L}_{\text{neck}}/R_{\text{neck}} - f_{\text{head}}R_{\text{head}}$  is minimized.<sup>3</sup> In order to insist conservation of membrane, we insert into the balance of forces the equation  $\mathcal{A} \approx 2\pi R_{\text{neck}}\mathcal{L}_{\text{neck}} + \mathcal{A}_{\text{head}}$  with  $\mathcal{A}$  a constant. Taken together, this results in the following implicit equation that we can solve for  $\mathcal{A}_{\text{head}}$ :

$$8\pi^2 \sqrt{\pi} K_b \left( \frac{\mathcal{L}_{\text{neck}}}{\mathcal{A} - \mathcal{A}_{\text{head}}} \right)^2 - f_{\text{head}}/\sqrt{\mathcal{A}_{\text{head}}} = 0. \quad (2)$$

Given numerical values of  $f_{\text{head}}, K_b, \mathcal{A}$  and  $\mathcal{L}_{\text{neck}}$ , solving equation (2) for  $\mathcal{A}_{\text{head}}$  returns all other geometrical quantities, e.g.  $R_{\text{neck}}, R_{\text{head}}$  and  $\mathcal{A}_{\text{neck}}$ . We have numerically solved this equation for a range of values for the total surface-area  $\mathcal{A}$  and number of actin filaments in the spine-head  $N = f_{\text{head}}/f_{\text{actin}}$ . The influences of *growth*, encoded in the total surface-area of the spine  $\mathcal{A}$ , and *cytoskeletal organization*, encoded in the number of actin filaments  $N$ , on spine morphology are combined in figure 3(d). Using equation (2) and solving for the radius of the spine-neck we find radii  $R_{\text{neck}} = 60 - 93$  nm (whereby we use estimates for the number of actin filaments  $N = 71$  and the typical surface-areas  $\mathcal{A} = 0.5 - 2.00 \mu\text{m}^2$ , cf. table 1). This range agrees quite well with the experimentally observed ranges  $R_{\text{neck}} = 45 - 105$  nm by [12] and  $R_{\text{neck}} = 50 - 100$  nm by [33]. From the similarity of these ranges, we infer that at least a substantial part of the force that is exerted by the actin filaments in the spine-head is directed towards counteracting the expansive force of the spine-neck. Moreover, given numerical values of the total surface-area of the spine  $\mathcal{A}$  we can solve for the number of actin filaments required for sustaining the spine-neck. We have done this for a wide range of surface-areas and reproduced the results in figure 3(b). These computations show that a larger spine-head (with the same total quantity of membrane) requires more actin filaments to sustain it. This is in agreement with findings by [8] that show that the number of actin filaments increases substantially with increasing surface-area. In fact, the datapoints published in [8] match our model for  $N(\mathcal{A}_{\text{head}})$  (see figure 3(c)). We have further used equation (2) for computing the ratios or radii  $R_{\text{head}}/R_{\text{neck}}$  and of volumes  $\mathcal{V}_{\text{head}}/\mathcal{V}_{\text{neck}}$ , shown in figure 3(c). We have found that both the numerical values of  $R_{\text{head}}/R_{\text{neck}}$  and the upward trend w.r.t.  $\mathcal{A}_{\text{head}}$  of this metric agree well with data published by [33] if we use for the number of actin filaments  $N \approx 70 - 150$ . Thus, the renders shown in figure 3(d) appear to be in the physiologically relevant regime. Moreover, this number for the actin filaments appears to be supported by empirical data that shows  $N \approx 50 - 150$  (we estimated this on the basis of data published in [8], see Supporting Information).

### 3.3 Relationship between Actin-Membrane Anchoring and Septin-Complexes on Spine Morphology

We have discussed possible links between the cytoskeleton and spine morphology and how, within our model, *pushing* the spine membrane at the location of the head effectively *pulls* the spine membrane

---

<sup>3</sup>We have shown by means of theoretical modeling and numerical simulations that we can neglect the force that is exerted by the contractile force due to the bending energy of the head. This fact is reflected in the small number of actin filaments required to sustain a large, bulbous head, as can be seen in figure 3(b).

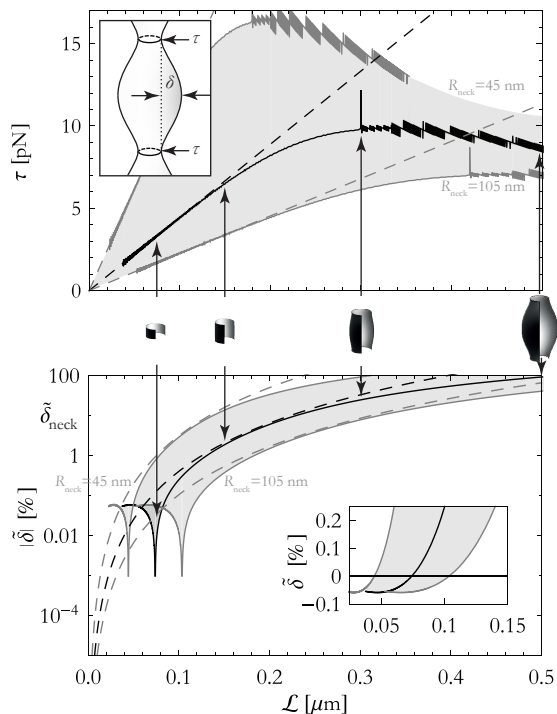


Figure 4: Results of simulations that have been performed using the energy functional (1) (solid curves) and theoretical model that treats these shapes as cylinders (dashed curves). The computations have been performed for  $R_{\text{neck}} = 45 \dots 105$  nm as indicated in the figure. Black lines corresponds to  $R_{\text{neck}} = 75$  nm. We used  $K_b = 5 \times 10^{-19}$  J for these computations [28]. Top panel: The line tension  $\tau$  as a function of the distance  $\mathcal{L}$  between the line tensions. Inset shows how line tension  $\tau$  and ‘unduloid amplitude’  $\delta$  are defined. Bottom panel: The absolute value of the reduced ‘unduloid amplitude’,  $|\tilde{\delta}|$ . Inset panel shows the reduced ‘unduloid amplitude’ where it crosses  $\tilde{\delta} = 0$ . Indicated is  $\tilde{\delta}_{\text{neck}} = 10\%$ , the approximate amplitude of variations in the width of the spine-neck, corresponding to  $\tau \approx 6.5 - 15$  pN.

inwards at the location of the spine-neck. Within our paradigm of the conservation of membrane, directly applying a contractile force  $\tau$  at one or more locations along the spine-neck can achieve the same result. This is possible due to the nature of the spine membrane, which can be regarded as a two-dimensional fluid—that is, contracting the spine-neck effectively channels membrane to the spine-head. Thus, applying a line tension can aid in the transition from an immature to a mature spine with a long, thin neck and bulbous head. Possible candidates for such line tensions are anchoring molecules (such as the WASP/WAVE network [2, 32]) septin-complexes that form ring-like structures [22] and spectrin [35]. Next, we will show that anchoring molecules or ring-like complexes are able to apply sufficient contractile force along the spine-neck.

A line tension can be included in our models by adding a term  $\tau\mathcal{C}$  to the Canham-Helfrich free energy (1), where  $\tau$  is the line tension and  $\mathcal{C} = 2\pi R_{\text{neck}}$  is the circumference of the spine-neck. The line tension can be measured thus  $\tau = -\partial\mathcal{E}/\partial\mathcal{C}$ , where  $\mathcal{E}$  is the bending energy of the shape. In figure 4 it can be seen that the line tensions are typically in the order of piconewtons. As a consequence of one or a number of such line tensions we find ‘unduloidal’ spine-necks. Some representative shapes along with the required line tension have been reproduced in figure 4. The shapes are characterized by an unduloid amplitude  $\delta$  which describes the maximum deviation from the base value  $R_{\text{neck}}$  (we have chosen to use the relative unduloid amplitude  $\tilde{\delta} = \delta/R_{\text{neck}}$ ).

Although we have not been able to find publications that measure the ‘unduloid amplitude’  $\tilde{\delta}$  for spine-necks, we have calculated this is in the order  $\sim 10\%$  or less (see Supplementary Information for details). Using this value of  $\tilde{\delta}$ , we find that—if line tensions are responsible for the typical spine-morphology—the line tensions need to be placed at distances of  $\mathcal{L} \approx 0.14 - 0.33 \mu\text{m}$ , as can be readily verified by examining figure 4. Then, computing the line tension (using numerical values  $R_{\text{neck}}$  and  $K_b$  from table 1) corresponding to  $\mathcal{L} \approx 0.14 - 0.33 \mu\text{m}$ , we find that each of the line tensions experiences a load of  $\tau \approx 6.5 - 15 \text{ pN}$ . This, too, can be verified by examining figure 4.

We are aware of various candidates for anchoring membrane to the cytoskeleton, such as L-selectin,  $\beta_2$  integrins and CD45. The literature reports that these three candidates have rupture forces respectively  $25 - 45 \text{ pN}$ ,  $60 - 120 \text{ pN}$  and  $35 - 85 \text{ pN}$  [29]. Even the lowest values of these three ranges is almost double our highest estimate for the required line tension. Therefore, it is safe to conclude that anchoring molecules can withstand the mechanical forces that are required in order to constrain the spine-neck to  $R_{\text{neck}} = 45 - 105 \text{ nm}$ .

Since spine-necks typically have lengths of  $0.2 - 2 \mu\text{m}$  (table 1, see Supporting Information), we find that the number of line tensions that needs to be placed is  $1 - 14$  (whereby we used the aforementioned distance between the line tensions  $\mathcal{L} \approx 0.14 - 0.33 \mu\text{m}$ ). However—as far as we can determine—literature does not mention these concentrations of anchoring molecules across all spine-necks. Although ring-like septin-complexes are found consistently along spine-necks [7, 22, 31], they are only reported to be positioned at the *base* of the spine and *not* along the full length of the spine-neck. Our models predict that it is required to place line tensions along the full length of the spine-neck in order to constrain it, and therefore we can refute septin-complexes as being solely responsible for constraining the long, thin spine-necks. Moreover, the assembly of septins into ring-like structures has an associated time-scale in the order of minutes [18]. Hence, we find that cytoskeletal remodeling—which can be performed on the time-scale of fractions of a second [21]—is much more rapid than positioning these constriction proteins.

## 4 Conclusions

We study the physical mechanisms that determine the morphology of dendritic spines. In particular, we investigate the ability of the actin cytoskeleton to change the size and shape of spines. We find that the most striking primary features of spine growth and spine morphology can be straightforwardly understood as a consequence of the trade-off between the elastic properties of the spine membrane and

the forces actively generated by the actin cytoskeleton. Specifically, we show that the initiation and formation of dendritic filopodia may be rationalized on the basis of the protrusive forces of the actin cytoskeleton. Using realistic estimates for the number of actin filaments involved, we find that the dimensions of the filopodia in our models agrees well with the observed dimensions of newly formed protrusions in the developing neuron.

We have also studied spine maturation, the process characterized by a morphological transition from a filopodium or thin spine to the mature mushroom-like spine. Using models based on the coupling between the actin cytoskeleton and the spine membrane, we find that the combined dynamics of branched actin and aligned actin inherently results in a mushroom-like morphology. Finally, we have discussed several candidate factors that might aid in the stabilization of the long, thin spine-neck and the bulbous spine-head. Our predictions for various morphological quantities, such as the neck radius  $R_{\text{neck}}$  and the ratios  $R_{\text{head}}/R_{\text{neck}}$  and  $\mathcal{V}_{\text{head}}/\mathcal{V}_{\text{neck}}$ , compare well with experimental data [12,33]. Furthermore, the suggested important dual roles of branched and aligned organizations suggest novel experiments analyzing (possibly, even, altering) the localization of proteins like Arp2/3 and septin to the spine head and neck. Summarizing, our model suggests that actin organization is autonomously capable of controlling the shape changes of dendritic spines, providing the forces and geometry support for both the initial filopodial stage and the mature mushroom-like shape.

## 5 Supporting Information

### 5.1 Estimate for the Number of Actin Filaments

We counted the number of actin filaments as 20 on  $\sim 20\%$  of the surface-area resulting in  $\sim 100$  filaments for one entire spine-head as published by [19]. Then, noting that *on the average* the filaments are not oriented perpendicular to the membrane—but rather at an angle  $\pi/4$ , we find the *effective* number of actin filaments to be  $\sim 100 \cdot \cos(\pi/4) \approx 71$ . This number falls within the range for the number of polymerizing filaments  $N = 50 - 150$  we derived from data published in [8] ([8] has published the density of non-stationary actin molecules, which we integrated over the surface area to obtain a measure for the number of polymerizing filaments).

### 5.2 Standard Deviation in Spine-Neck Width

We measured the width of the spine-neck of images by [33] by fitting the intensity of the profile with Gaussian distributions along the axis of the spine-neck. We asserted that the standard deviation of these Gaussians is a measure for the width of the spine-neck. Then, we computed the relative variation in these widths. Using this method, the relative variation in the width of the spine-neck was found to be 13.5%.

### 5.3 Shape Equations

Taking the first variation of the Canham-Helfrich energy functional (1), and insisting that the first variation  $\delta\mathcal{E}$  is zero under all possible infinitesimal perturbations results in a differential equation that describes stationary shapes  $\{r(s), \psi(s)\}$ .<sup>4</sup> This differential equation, that we shall henceforth call the

---

<sup>4</sup>The stationary shapes include shapes corresponding to an energetic minimum, an energetic maximum or a saddle point in the energy functional. A seminal paper by [38] describes the higher-order variations, from which we can infer the class of stationary point. We will not discuss this technical difficulty in this publication, although we have used numerical perturbative methods to determine which shapes correspond to energetic minima.

shape equation, is [3, 16, 20]

$$\psi^{(3)} = -\frac{1}{2}(\psi')^3 - \frac{2 \cos \psi}{r} \psi'' + \frac{3 \sin \psi}{2r} (\psi')^2 + \frac{\bar{\sigma}}{r} \sin \psi + \frac{3(\cos \psi)^2 - 1}{2r^2} \psi' + \bar{\sigma} \psi' - \frac{(\cos \psi)^2 + 1}{2r^3} \sin \psi, \quad (3)$$

where we have dropped the  $s$ -dependencies and  $\bar{\sigma} \equiv \sigma/K_b$ . Most publications that we have consulted make reference to second-order shape equations [16], but—in accordance with [3]—we find the third-order shape equation (3) to be numerically substantially more stable. The second-order shape equations, e.g. found by taking the first integral of (3), is used to find boundary conditions for  $\psi''$ . This equation is [3]

$$\psi'' \cos \psi = -\frac{1}{2}(\psi')^2 \sin \psi - \frac{(\cos \psi)^2}{r} \psi' + \frac{(\cos \psi)^2 + 1}{2r^2} \sin \psi + \bar{\sigma} \sin \psi - \frac{\bar{f}}{r}, \quad (4)$$

where  $\bar{f} \equiv f/K_b$ . Although the point force  $f$  does not show up in the shape equation (3), it does enter in the determination of the correct boundary conditions through (4).

We use a shooting-and-matching algorithm (for more information on this numerical technique, we refer to [13]) whereby  $\psi'(0)$ ,  $f$ ,  $\sigma$  are used as shooting variables.

## References

- [1] B. Angelov and I. M. Mladenov. On The Geometry of Red Blood Cell. *Proceedings of the First International Conference on Geometry, Integrability and Quantization*, pages 27–46, 2000.
- [2] G. G. Borisy and T. M. Svitkina. Actin machinery: pushing the envelope. *Current Opinion in Cell Biology*, 12(1):104–112, feb 2000.
- [3] I. Derenyi, F. Julicher, and J. Prost. Formation and interaction of membrane tubes. *Physical review letters*, 88(23):238101, 2002.
- [4] A. Diz-Munoz, D. A. Fletcher, and O. D. Weiner. Use the force: membrane tension as an organizer of cell shape and motility. *Trends in cell biology*, 23(2):47–53, feb 2013.
- [5] F. Engert and T. Bonhoeffer. Dendritic spine changes associated with hippocampal long-term synaptic plasticity. *Nature*, 399(6731):66–70, 1999.
- [6] J. F. Evers, D. Muench, and C. Duch. Developmental relocation of presynaptic terminals along distinct types of dendritic filopodia. *Developmental biology*, 297(1):214–27, sep 2006.
- [7] H. Ewers, T. Tada, J. D. Petersen, B. Racz, M. Sheng, and D. Choquet. A Septin-Dependent Diffusion Barrier at Dendritic Spine Necks. *PLoS ONE*, 9(12):e113916, 2014.
- [8] N. A. Frost, H. Shroff, H. Kong, E. Betzig, and T. A. Blanpied. Single-molecule discrimination of discrete perisynaptic and distributed sites of actin filament assembly within dendritic spines. *Neuron*, 67(1):86–99, jul 2010.
- [9] N. C. Gauthier, T. A. Masters, and M. P. Sheetz. Mechanical feedback between membrane tension and dynamics. *Trends in cell biology*, 22(10):527–35, oct 2012.

- [10] K. M. Harris, F. E. Jensen, and B. Tsao. Three-dimensional structure of dendritic spines and synapses in rat hippocampus (CA1) at postnatal day 15 and adult ages: implications for the maturation of synaptic physiology and long-term potentiation. *The Journal of neuroscience : the official journal of the Society for Neuroscience*, 12(7):2685–2705, 1992.
- [11] K. M. Harris and J. K. Stevens. Dendritic spines of rat cerebellar Purkinje cells: serial electron microscopy with reference to their biophysical characteristics. *The Journal of neuroscience : the official journal of the Society for Neuroscience*, 8(12):4455–4469, 1988.
- [12] K. M. Harris and J. K. Stevens. Dendritic Spines of CA1 Pyramidal Cells in the Rat Hippocampus : Serial Electron Microscopy with Reference to Their Biophysical Characteristics. *Journal of Neuroscience*, 9(8):2982–2997, 1989.
- [13] M. T. Heath. *Scientific Computing: An Introductory Survey*. McGraw-Hill, 2002.
- [14] P. Hotulainen and C. C. Hoogenraad. Actin in dendritic spines: Connecting dynamics to function. *Journal of Cell Biology*, 189(4):619–629, may 2010.
- [15] F. Julicher and R. Lipowsky. Shape transformations of vesicles with intramembrane domains. *Physical Review E*, 53(3):2670–2683, 1996.
- [16] F. Julicher and U. Seifert. Shape equations for axisymmetric vesicles: A clarification. *Physical Review E*, 49(5):4728–4731, 1994.
- [17] H. Kasai, M. Fukuda, S. Watanabe, A. Hayashi-Takagi, and J. Noguchi. Structural dynamics of dendritic spines in memory and cognition. *Trends in Neurosciences*, 33(3):121–129, 2010.
- [18] M. Kinoshita, C. M. Field, M. L. Coughlin, A. F. Straight, and T. J. Mitchison. Self- and Actin-Templated Assembly of Mammalian Septins. *Developmental Cell*, 3(6):791–802, dec 2002.
- [19] F. Korobova and T. Svitkina. Molecular architecture of synaptic actin cytoskeleton in hippocampal neurons reveals a mechanism of dendritic spine morphogenesis. *Molecular biology of the cell*, 21(1):165–176, 2010.
- [20] J. Mathews. *Axisymmetrical equilibrium shapes of two-phase biological membranes*. PhD thesis, 2012.
- [21] A. Mogilner and G. Oster. Force generation by actin polymerization II: the elastic ratchet and tethered filaments. *Biophysical journal*, 84(3):1591–1605, 2003.
- [22] S. Mostowy and P. Cossart. Septins: the fourth component of the cytoskeleton. *Nature Reviews Molecular Cell Biology*, 13, 2012.
- [23] K.-I. Okamoto, T. Nagai, A. Miyawaki, and Y. Hayashi. Rapid and persistent modulation of actin dynamics regulates postsynaptic reorganization underlying bidirectional plasticity. *Nature Neuroscience*, 7(10):1104–1112, sep 2004.
- [24] M. Park, J. M. Salgado, L. Ostroff, T. D. Helton, C. G. Robinson, K. M. Harris, and M. D. Ehlers. Plasticity-Induced Growth of Dendritic Spines by Exocytic Trafficking from Recycling Endosomes. *Neuron*, 52(5):817–830, 2006.
- [25] D. Raucher and M. P. Sheetz. Characteristics of a membrane reservoir buffering membrane tension. *Biophysical journal*, 77(4):1992–2002, oct 1999.
- [26] W. Rawicz, K. C. Olbrich, T. McIntosh, D. Needham, and E. Evans. Effect of chain length and unsaturation on elasticity of lipid bilayers. *Biophysical journal*, 79(1):328–339, 2000.

- [27] U. Seifert. Configurations of fluid membranes and vesicles. *Advances in Physics*, 46(1):13–137, 1997.
- [28] S. Semrau, T. Idema, L. Holtzer, T. Schmidt, and C. Storm. Accurate Determination of Elastic Parameters for Multicomponent Membranes. *Physical Review Letters*, 100(8):088101, feb 2008.
- [29] J. Y. Shao and R. M. Hochmuth. Mechanical anchoring strength of L-selectin, beta2 integrins, and CD45 to neutrophil cytoskeleton and membrane. *Biophysical journal*, 77(1):587–596, 1999.
- [30] M. Stone and P. Goldbart. *Mathematics For Physics*. Cambridge University Press, 2012.
- [31] T. Tada, A. Simonetta, M. Batteredton, M. Kinoshita, D. Edbauer, and M. Sheng. Role of Septin Cytoskeleton in Spine Morphogenesis and Dendrite Development in Neurons. *Current Biology*, 17(20):1752–1758, 2007.
- [32] T. Takenawa and S. Suetsugu. The WASP-WAVE protein network: connecting the membrane to the cytoskeleton. *Nature Reviews Molecular Cell Biology*, 8(1):37–48, jan 2007.
- [33] J. Tonnesen, G. Katona, B. Rózsa, and U. V. Nägerl. Spine neck plasticity regulates compartmentalization of synapses. *Nature neuroscience*, 17(5):678–85, 2014.
- [34] Z. Wang, J. G. Edwards, N. Riley, D. W. Provan, R. Karcher, X. D. Li, I. G. Davison, M. Ikebe, J. a. Mercer, J. a. Kauer, and M. D. Ehlers. Myosin Vb Mobilizes Recycling Endosomes and AMPA Receptors for Postsynaptic Plasticity. *Cell*, 135(3):535–548, 2008.
- [35] K. Xu, G. Zhong, and X. Zhuang. Actin, spectrin, and associated proteins form a periodic cytoskeletal structure in axons. *Science (New York, N.Y.)*, 339(6118):452–6, jan 2013.
- [36] G. Yang, F. Pan, and W.-B. Gan. Stably maintained dendritic spines are associated with lifelong memories. *Nature*, 462(7275):920–924, 2009.
- [37] N. Yasumatsu, M. Matsuzaki, T. Miyazaki, J. Noguchi, and H. Kasai. Principles of long-term dynamics of dendritic spines. *The Journal of neuroscience : the official journal of the Society for Neuroscience*, 28(50):13592–13608, dec 2008.
- [38] O. Y. Zhong-Can and W. Helfrich. Bending energy of vesicle membranes: General expressions for the first, second, and third variation of the shape energy and applications to spheres and cylinders. *Physical Review A*, 39(10):5280–5288, may 1989.
- [39] N. E. Ziv and S. J. Smith. Evidence for a Role of Dendritic Filopodia in Synaptogenesis and Spine Formation. *Neuron*, 17(1):91–102, jul 1996.